First-principles Calculations of the Electronic Structure and Optical Properties of Graphene-like In$_x$Al$_{1-x}$N Monolayers

Xuewen WANG [*], **Yanbo ZHAO, Haiting BAI, Yuanmeng ZHANG, Jie GAO, Chunxue ZHAI, Yang DAI**

School of Information Science and Technology, Northwest University, Xi'an City, China, 710127

crossref http://dx.doi.org/10.5755/j02.ms.30035

This paper employs the Heyd-Scuseria-Ernzerhof (HSE) function to research electronic structures of monolayer In$_x$Al$_{1-x}$N with different compositions (x = 0, 0.25, 0.5, 0.75, 1) based on the first-principles, and the optical properties of single-layer In$_x$Al$_{1-x}$N are calculated by Generalized Gradient Approximation-Perdew Burke Ernzerhof (GGA-PBE) function. The influence of the electronic structure on the properties has been analyzed. Then the influence of doping quantity on the characteristics has been summarized, which also indicates the trend of the complex dielectric function and absorption spectrum. The calculation results show that with the increase of x, the static dielectric constant increases, the electron transition ability increases, and the absorption peak intensity in the light absorption spectrum increases. It can conclude that the In$_x$Al$_{1-x}$N compound can theoretically achieve the adjustable Eg and photoelectric performance with x, which will apply in making various optoelectronic devices, including solar cells and sensors.

Keywords: In$_x$Al$_{1-x}$N, density functional theory, electronic structure, photoelectric property.

1. INTRODUCTION

The ever-growing electronic technology has InN-based semiconductor materials (such as binary InN or ternary InGaN crystals) that belong to direct gap semiconductors attracted extensive attention. They are favorable electronic and optical properties, including high carrier mobility, high breakdown voltage, high speed, and a considerable range of emissions in the visible spectrum [1]. There makes it possible to widely use in power electronic equipment, sensors, high-efficiency solar cells, high electron mobility transistors (HEMT), and other fields [2, 3]. As an III-V nitride semiconductor, In$_x$Al$_{1-x}$N has a large and adjustable bandgap ranging from 0.7 eV to 6.2 eV [4], as well as excellent photoelectric properties, so it has become a current research hotspot.

In the process of the experiment, In$_x$Al$_{1-x}$N materials preparation is difficult due to a very discrepancy in the growth environment between the InN and the AlN. As their material thickness can be controllable theoretically, many scholars have researched III-V nitride semiconductors through theoretical calculations. As early as 1986, Ching W Y and others used first principles to calculate the AlN of electronic structure, lattice constant, internal parameters, and cohesive energy. Subsequently, researchers applied first-principles calculations to the thermodynamic and electronic properties of In$_x$Al$_{1-x}$N alloys [5,6] research. They also studied the thermodynamic stability and charger distribution of ternary AlGaN, InGaN, and InGaN alloys [7]. In recent years, some scholars have also studied the III-V nitrides' [8] elastic properties, adsorption properties [9, 10], and changes in band gap and magnetic properties caused by their defects [11, 12]. At the same time,

researchers have also considered changing their composition or modifying through doping and compounding methods to explore III-V nitride materials' electronic structure and other properties [13 – 15].

In recent years, international articles on III-V nitride semiconductors are more about binary compounds AlN, InN, GaN [16 – 20], and most of the research on In$_x$Al$_{1-x}$N mainly explores its bulk materials and multilayer film [21, 22]. However, the first-principles study on the electronic structure and optical properties of the nano-scale graphene-like monolayer In$_x$Al$_{1-x}$N rare discusses. And for the optical properties, the DFT framework is not accurate enough because of the underestimation of the bandgap. By employing Heyd-Scuseria-Ernzerhof (HSE) function based on the first-principles that is more accurate than DFT, this paper discusses the electronic structure and optical properties of the graphene-like monolayer In$_x$Al$_{1-x}$N. The paper also exhaustively discusses optoelectronic properties of monolayer In$_x$Al$_{1-x}$N with different compositions, which provides an important theoretical basis for the research of optoelectronic devices and sensors.

2. MODEL AND COMPUTATIONAL METHODS

2.1. Model establishment

AlN and InN are both III-V binary nitrides. The space group is 186 (p63mc), the crystal plane axis angle is $\alpha = \beta = 90°, \gamma = 120°$. The lattice constants of AlN [23] are $a = b = 3.11$ Å, $c = 4.98$ Å, and the lattice constants of InN are $a = b = 3.544$ Å, $c = 5.718$ Å. As shown in Fig. 1, along with the cutting direction of 001, the constructed AlN

---

[*] Corresponding author. Tel.: +13488466766.

E-mail address: *wangxuew@nwu.edu.cn* (X. Wang)

and InN unit cells cut into a monolayer unit cell, which contains one Al (In) atom and one N atom.
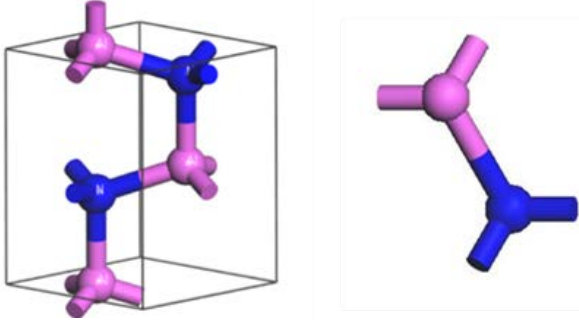

Fig. 1. AlN unit cell and cut monolayer unit cell

As shown in Fig. 2, the $In_xAl_{1-x}N$ model, AlN, and InN belong to III-V nitrides, all of which are wurtzite structures. In this paper, based on the optimized AlN unit cell, we select a $4 \times 4 \times 1$ supercell model and set the vacuum layer to 15 Å. Specifically, there are 32 atoms, 16 Al atoms, and 16 N atoms in the AlN monolayer. On this basis, In atoms are introduced to replace Al atoms in AlN to construct $In_xAl_{1-x}N$ supercells. According to Fig. 2, it can be concluded that when the exponent increases, one Al atom is uniformly replaced with In atoms of each oblique column.
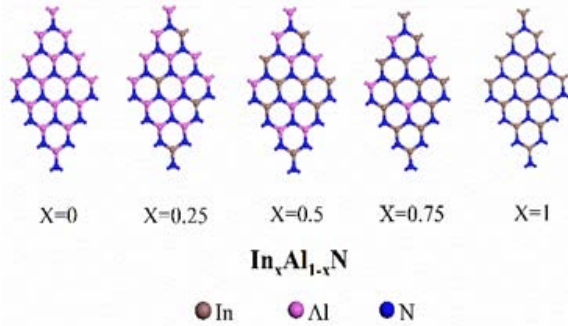

Fig. 2. $In_xAl_{1-x}N$ models

2.2. Calculation method

The structure optimization and performance calculations in this paper are all carried out in the Cambridge Serial Total Energy Package (CASTEP) module of Material Studio software. To ensure the accuracy of the data, the experiment first conducts interactive functional, cut-off energy, and K-point tests on AlN and InN monolayer unit cell structures. In the CASTEP module, the Medium is for optimization and the Fine for calculation. Generalized Gradient Approximation-Perdew Burke Ernzerhof (GGA-PBE) functions describe the interaction between electrons and ions using super soft pseudopotentials [24], and the Two-Point Steepest Descent (TPSD) algorithm is employed in the model optimization process. The energy convergence precision is 1.0×10^{-5} eV/atom, the stress convergence precision is 0.05 GPa, the displacement convergence precision is 1.0×10^{-3} Å, and the force convergence precision is 0.03 eV/Å. In the monolayer calculation of $In_xAl_{1-x}N$, the integration path in $G(0,0,0)$-$M(0,0.5,0)$-$K(-0.333,0.667,0)$-$G(0,0,0)$, which is involved the valence electrons are In: $4d^{10}5s^25p^1$, Al: $3s^23p^1$, N: $2s^22p^3$.

3. RESULTS AND DISCUSSION

3.1. Analysis of the electric structure of $In_xAl_{1-x}N$ crystal

3.1.1. Geometric structure and stability analysis

After geometrically optimizing the $4 \times 4 \times 1$ supercell, the lattice constant and bond length of the supercell change slightly. To understand the stability of the monolayer structure, it is necessary to consider the binding energy E_b. Therefore, this part analyzes the stability of five monolayer structures from the energy point of view. Specifically, the energy is the binding energy released when the particles combine to form new particles. The larger the calculated absolute value of the energy is, the more stable the system is. The specific expression is [25]:

$$E_b = \frac{1}{N}\{E_t - n_0 E_i(In) - n_1 E_i(N) - n_2 E_i(Al)\}. \quad (1)$$

Among them, E_t represents the total energy of the $In_xAl_{1-x}N$ monolayer structure system. The energy of the three atoms of In, Al, and N in the free state is represented by $E_{isolate}$ (In), $E_{isolate}$ (Al), $E_{isolate}$ (N), and n_0 are In in the system. And n_1 is the total number of N atoms in the system, n_2 is the number of Al atoms in the system. Therefore, the specific formula for the $In_xAl_{1-x}N$ monolayer system when x is equal to 0.5 is:

$$E_b = \frac{1}{32}\{E_t - 8E_i(Al) - 16E_i(N) - 8E_i(In)\}. \quad (2)$$

In the analysis of structure and stability, this paper respectively lists a(Å) lattice constant, dIn-N (which is the bond length between In atom and N atom), and dAl-N (which is the bond length and binding energy between Al atom and N atom). The measurement and calculation results are shown in Table 1. After calculating by GGA, the obtained lattice constants of InN and AlN are larger than the experimental values. Among them, the deviation of AlN and the experimental value is 0.25 %, and the deviation of InN is 1.3 %. Since the In^{3+} ion radius is larger than the Al^{3+} ion radius, with the increase of x, the lattice constant of the supercell gradually increases, and the volume of the supercell also increases when the Al in the AlN monolayer is doped with In instead of substitution, which is in line with Vegard`Law [26]. The bond length of AlN and InN are consistent with those in reference [27]. The binding energies of the five systems are all negative, indicating that the five models are all thermodynamically stable configurations with a certain degree of stability. Compared with InN, AlN has better stability, and the structure becomes more stable as the In composition increases. The absolute value of binding energy decreases.

Table 1. The theoretical values of lattice constant, bond length and binding energy of $In_xAl_{1-x}N$ monolayer were optimized

	a(Å)	d_{In-N}	d_{Al-N}	E_b
AlN	12.51	–	1.800	-5.56
$In_{0.25}Al_{0.75}N$	12.93	2.054	1.781	-6.44
$In_{0.5}Al_{0.5}N$	13.45	2.074	1.820	-5.92
$In_{0.75}Al_{0.25}N$	13.92	2.078	1.820	-5.42
InN	14.35	2.073	–	-5.04

By calculating the frequency values of phonons of $In_{0.5}Al_{0.5}N$ structure at the special points G (0.0,0.0,0.0), Y (0.0,0.5,0.0) and, D (0.5,0.0,0.5) in the Brillouin region, the experiment obtains the curves of phonon dispersion and density of states, as shown in Fig. 3 a.
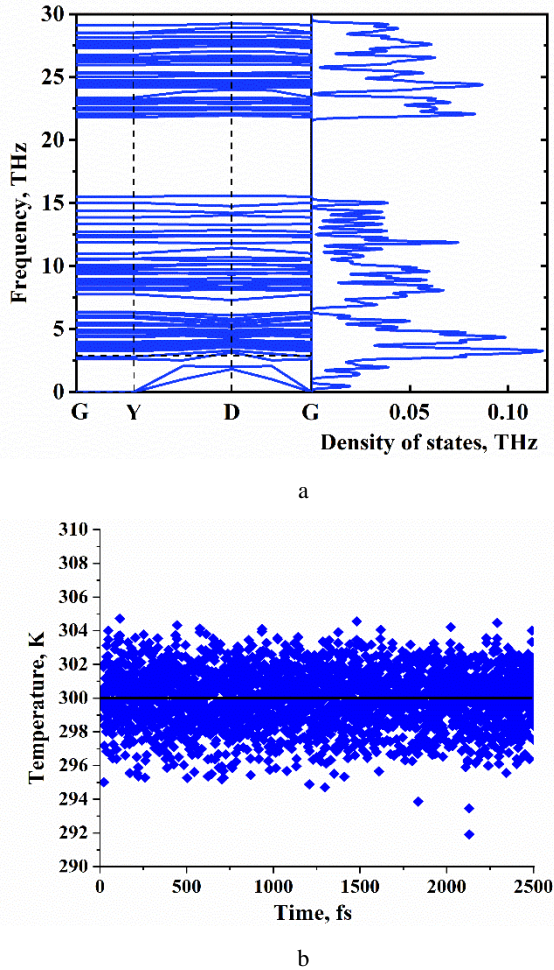

a

b

Fig. 2. a – the curves of phonon dispersion and density of states, b – temperature fluctuation curve of dynamic relaxation

If the protocell contains N atoms, the dispersion relationship should involve 3N branches, including 3 acoustic branches and 3N-3 optical branches. The single layer $In_{0.5}Al_{0.5}N$ contains 32 atoms, so there should be 3 acoustic branches and 93 optical branches. This calculated result is just consistent with the theory. It can be seen that from this figure that there is an obvious bandgap in the structure (i.e. the phonon frequency in this range is zero), and the range is approximately 15 – 22 THz. This result can be explained by the large difference in the relative mass of the atoms constituting the structure. The phonon dispersion curve shows that there is no obvious virtual frequency near the center of the Brillouin region, which indicates that the parameter setting of structural optimization is reasonable, and the structure is relatively stable theoretically. At the same time, we also carry out MD molecular dynamics calculations for the geometrically optimized $In_{0.5}Al_{0.5}N$ model. The whole system is simulated under NVT ensemble (the energy E is not fixed, but the temperature T and volume V have definite values) with periodic boundary conditions, the time step sets to 1fs, the simulation time is 2.51ps, and

the temperature sets to 300 K. As shown in Fig. 3 b, during NVT operation, the temperature fluctuates in a small range ($\pm$ 10 ℃) near 300 K. In the process of kinetic relaxation, when the fluctuation amplitude is less than 10 %, the system has reached a relatively stable state. Referring to this standard, it can conclude that this system is already in a relatively stable state.

3.1.2. Analysis of energy band and density of states

Due to the change of electron energy, an energy band makes a transition in energy level. For semiconductors, when external conditions change, part of the electrons in the full band absorb energy from the external electric field and transition to the empty band with not occupied by electrons and then form current, which is called the conduction band. Valence band maximum (VBM) is the top of the valence band, E_g called the forbidden bandwidth, and conduction band minimum (CBM) is the low conduction band. Band analysis is generally one of the first-principles works of analyzing materials.

Fig. 4 shows the energy band structure of $In_xAl_{1-x}N$ ($x = 0, 0.25, 0.5, 0.75, 1$) and the corresponding density of states diagram. Fig. 4 f summarizes the variation of the $In_xAl_{1-x}N$ monolayer varies with x, and numbers at points of graph line indicate the forbidden bandwidth of different x. When $x = 0$, it is a $4 \times 4 \times 1$ monolayer AlN model. As can be seen, in (a), the forbidden bandwidth of the monolayer AlN is 2.561 eV, and CBM and the VBM are at different points in the Brillouin zone, so it is an indirect bandgap semiconductor. The conduction band ranges from 2.561 eV to 15.4 eV, and the valence band is mainly composed of an upper valence band from 0 eV to -4.83 eV. The result is similar to the energy band of AlN In [9].

When $x = 1$, it is a monolayer InN model, as shown in Fig. 4 e. Its bandgap is 1.936 eV. The low conduction band and the top of the valence band locate at different positions in the Brillouin zone, so it is an indirect bandgap semiconductor. The conduction band ranges from 1.936 eV to 17.8 eV, and the valence band is composed of an upper valence band from 0 eV to -5.03 eV and a lower valence band from -10.6 eV to -14.7 eV. Compared with the energy band of the conduction band and the two valence bands, the effective mass of electrons in the conduction band is smaller than the other two energy bands, and there is a forced degree of non-locality and atomic orbital extensibility.

The experimental values of the $In_xAl_{1-x}N$ bandgap width of different components are shown in Table 2 [4]. Both theoretical and experimental results show that, with the decrease of x, the forbidden bandwidth of $In_xAl_{1-x}N$ gradually decreases, which is in line with Vegard's Law.

Table 2. Experimental values of $In_xAl_{1-x}N$ bandgap width of different components

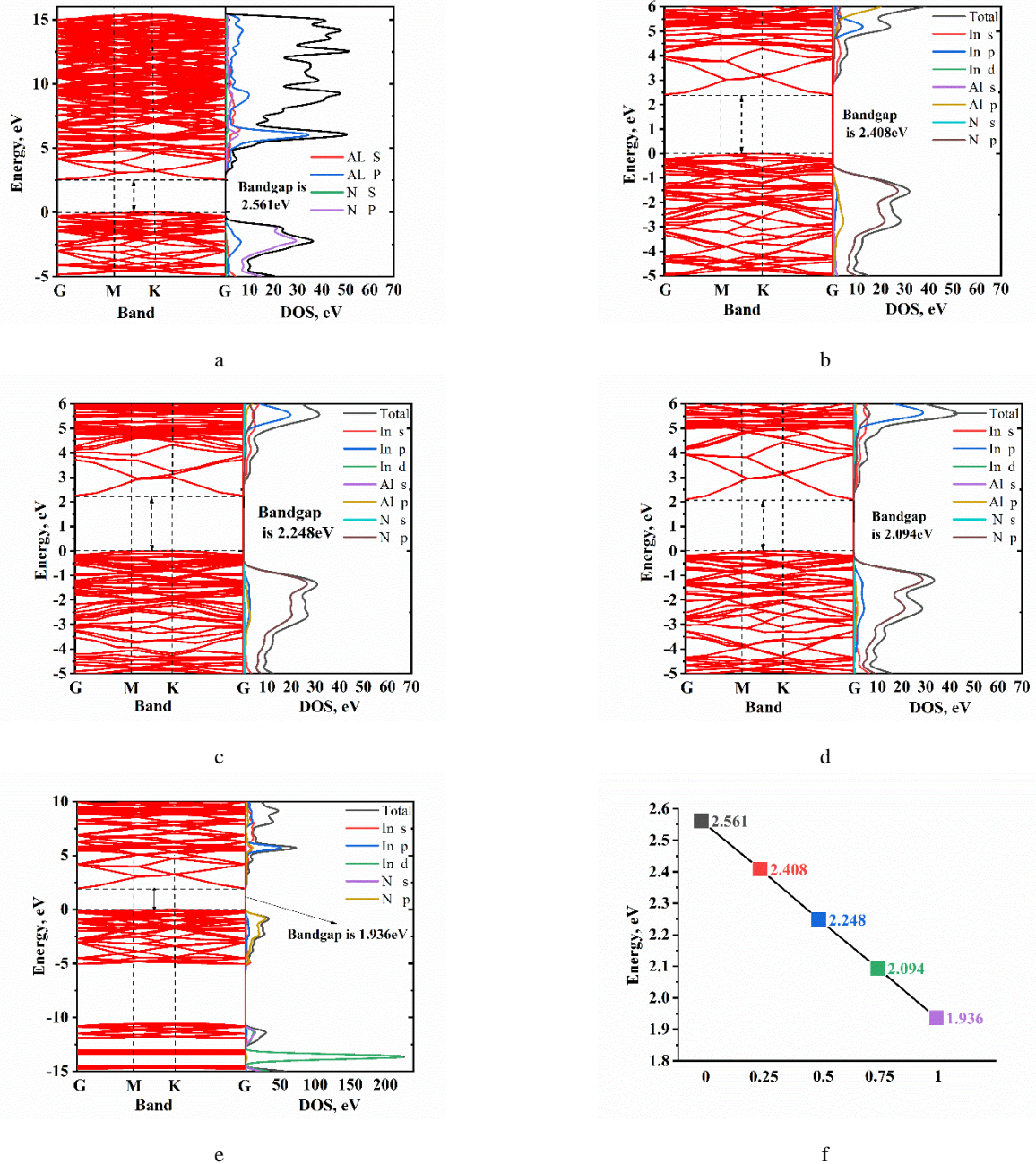| $In_xAl_{1-x}N$	E_g, eV
AlN	6.3
$In_{0.54}Al_{0.46}N$	1.93
$In_{0.55}Al_{0.45}N$	1.88
$In_{0.58}Al_{0.42}N$	1.69
$In_{0.61}Al_{0.39}N$	1.60
$In_{0.64}Al_{0.36}N$	1.47
$In_{0.67}Al_{0.33}N$	1.35
InN	0.7

Fig. 4. a, b, c, d, e – band structure of In$_x$Al$_{1-x}$N (x = 0, 0.25, 0.5, 0.75, 1) and the corresponding density of states diagram; f – bandgap of In$_x$Al$_{1-x}$N (x=0,0.25,0.5,0.75,1) monolayer

By adjusting the compositions of In and Al, it realizes the monolayer bandgap of the In$_x$Al$_{1-x}$N between AlN and InN.

The monolayer bandgap is directly and continuously adjustable, which reflects the application of In$_x$Al$_{1-x}$N materials in optical devices ranging from visible light to ultraviolet light.

The density of states can be combined with the energy band structure to analyze the energy state structure of electrons in a solid, and explain the distribution of electrons in a certain energy range and the distribution of electrons in each orbit. The density of states has two forms: partial density of states (PDOS) and total density of states (TDOS), which can better explain the interaction between atoms and

help us better analyze nano-scale solid semiconductor materials. Fig. 4 shows the five energy bands and density of states structure diagrams of In$_x$Al$_{1-x}$N (x = 0, 0.25, 0.5, 0.75, 1). Because their model structures and calculation methods are similar to the others, we only analyze in the case of x = 0, 0.5, 1. Fig. 4 a shows the TDOS and PDOS of the AlN monolayer. It can be seen from the figure that the conduction band and the upper valence band are mainly contributed by Al 3s, Al 3p, and N 2p states, and the p orbital contribution is greater. The peak at 5.8 eV is mainly contributed by Al 3p, the peak at -1.3 eV is mainly contributed by N 2p and the lower valence band is mainly contributed by N 2s. Fig. 4 c gives the DOS diagram of the In$_{0.5}$Al$_{0.5}$N monolayer.

The conduction band is mainly composed of In 5p and Al3p, which is similar to AlN. The p-orbital contributes more to it and is wider than other energy ranges, which is consistent with the energy band results. The lower valence band is mainly composed of In 4d and N 2s, and the peak at -13 eV is mainly contributed by In 4d. Fig. 4 e is the DOS diagram of the InN monolayer. The conduction band is mainly composed of N 2p, In 5s, and In 5p, while the upper valence band is mainly composed of N 2p and In 5s, and the lower valence band is mainly composed of N 2s and In 4d. The peak of -13 eV is mainly contributed by In. As the In composition increases, the peak value of the total density of states between -10 eV and -15 eV becomes stronger, which is mainly contributed by In 4d. As shown in Fig. 4 f, the forbidden bandwidth of the material also shows a linearly decreasing trend with the increase of the In composition, which shows that the bandgap of the $In_xAl_{1-x}N$ monolayer can be adjusted between the range of AlN and InN. The realization of the characteristics of direct and continuous adjustment also shows that $In_xAl_{1-x}N$ materials can be applied to optical devices ranging from visible light to ultraviolet light.

3.2. Discussion on the calculation characteristics of $In_xAl_{1-x}N$ crystal

We often use the optical properties of semiconductors to discuss the light absorption and the optoelectronic properties of materials. The essence of the optical properties of the material is the interaction of photons, electrons, and atoms in the material. The equation function which

describes the light absorption by the complex dielectric is [28]:

$$\varepsilon(\omega) = \varepsilon_1(\omega) \div i\varepsilon_2(\omega); \tag{3}$$

$$N(\omega) = n(\omega) \div ik(\omega). \tag{4}$$

Among them, $\varepsilon(\omega)$ is the complex dielectric function, ε_2 is the imaginary part, ε_1 is the real part, and N is the complex refractive index function. $n(\omega)$ is the real refractive index, and $k(\omega)$ is the extinction coefficient. Use the relationship between N and complex permittivity [29]:

$$(n(\omega) + ik(\omega))^2 = \varepsilon_1(\omega) + \varepsilon_2(\omega). \tag{5}$$

According to the Kramers–Kronig relations between $n(\omega)$ and $k(\omega)$, the absorption coefficient $\alpha(\omega)$ can be obtained [30]:

$$\alpha(\omega) = \frac{2\omega k(\omega)}{C} = \frac{\varepsilon_2(\omega)\omega}{n(\omega)C}. \tag{6}$$

The above formulas are the basic theory of optical properties, and these parameters can better describe the microscopic properties of materials.

3.2.1. Complex dielectric function

Fig. 5 a depicts the imaginary part of the dielectric function of the monolayer $In_{1-x}Al_xN$. There are multiple peaks in the whole energy spectrum, which correspond to the light absorption of multiple energy electron transitions, and the main peak is formed by the transition of N 2p state from the valence band to the conduction band.
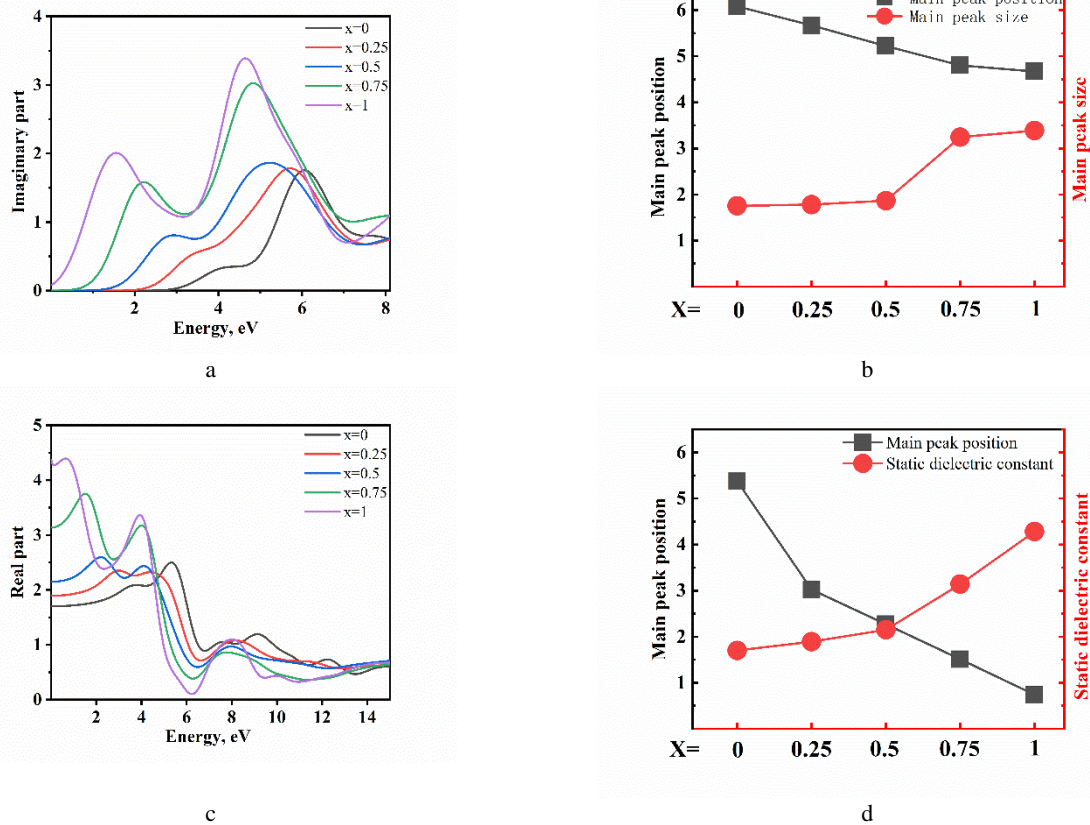

Fig. 5. The imaginary and real parts of the dielectric function and its changing law

Fig. 5 b shows the changing trend of the main peak position from 6.08 eV to 4.67 eV when the aluminum concentration increases from 0 % to 100 %. When the concentration of Al increases from 0 % to 100 %, the position of the main peaks moves in the direction of low energy without any notable shape changes, which is in good agreement with the decrease of the bandgap. It shows that the transition ability of the $In_{1-x}Al_xN$ electron is higher than AlN. The reason is that with the increase of x, the overlap and hybridization degree of in 4d and N 2S increase, resulting in the gradual decrease of E_g and the enhancement of electron transition ability. Fig. 5 c is the real part of the complex dielectric function. Observation shows that the vibration frequencies of the five lines show a significantly similar change trend, and finally reach a plateau. Fig. 5 d summarizes that with the gradual increase of the In composition, The main peaks are located at 5.37, 3.02, 2.27, 1.51, and 0.74 respectively, the peaks move to the low-energy direction. The static dielectric constant of the material is the value corresponding to the ordinate when the energy is 0 eV in Fig. 5 c. Fig. 5 d shows that the static dielectric constants of $In_xAl_{1-x}N$ (x = 0, 0.25, 0.5, 0.75, 1) are 1.7, 1.89, 2.15, 3.14, 4.28, respectively. With the increase of In composition, the static dielectric constant gradually increases. The explanation for this phenomenon is that the band gap decreases with the In increases, which makes it easier for electrons to transition from the top of the valence band to the low conduction band, so the static dielectric constant becomes larger.

3.2.2. Light absorption and loss

It can be seen from Fig. 6 a the light absorption diagram of $In_xAl_{1-x}N$ monolayer that the absorption edges of $In_xAl_{1-x}N$ monolayer AlN, $In_{0.25}Al_{0.75}N$, $In_{0.5}Al_{0.5}N$, $In_{0.75}Al_{0.25}N$, and InN are respectively 2.89 eV, 2.24 eV, 1.58 eV, 0.98 eV, 0.48 eV. Redshift occurs with the increase of In composition, and electrons in the material are more likely to process a transition from the valence band to the conduction band (Fig. 5 c).

The spectral range is mainly within 4 eV – 18 eV, corresponding to the blue-violet light band between 100 nm – 400 nm. In the monolayer $In_xAl_{1-x}N$ material, the absorption peak of InN is the highest, and the peak of AlN is the lowest. With the gradual increase of the In composition, the absorption peak intensity of the one-dimensional $In_xAl_{1-x}N$ material gradually increases. It indicates that the In composition with the introduction of light absorption improves the luminous performance of $In_xAl_{1-x}N$. Fig. 6 b is the light loss function of the $In_xAl_{1-x}N$ monolayer.

Compared with Fig. 6 a, the curve shows a similar trend development, indicating that the absorption is proportional to the loss. The monolayer $In_xAl_{1-x}N$ material gradually decreases with the x increases. The peak position of the highest loss peak gradually reduces, located at 13.5 eV, 12.6 eV, 11.9 eV, 11.7 eV, 11.4 eV, and progressively moves towards the lower energy direction, as shown in Fig. 6 c. The calculation results show that the introduction of In component improves both the light absorption of the material and the luminescence performance of $In_xAl_{1-x}N$.
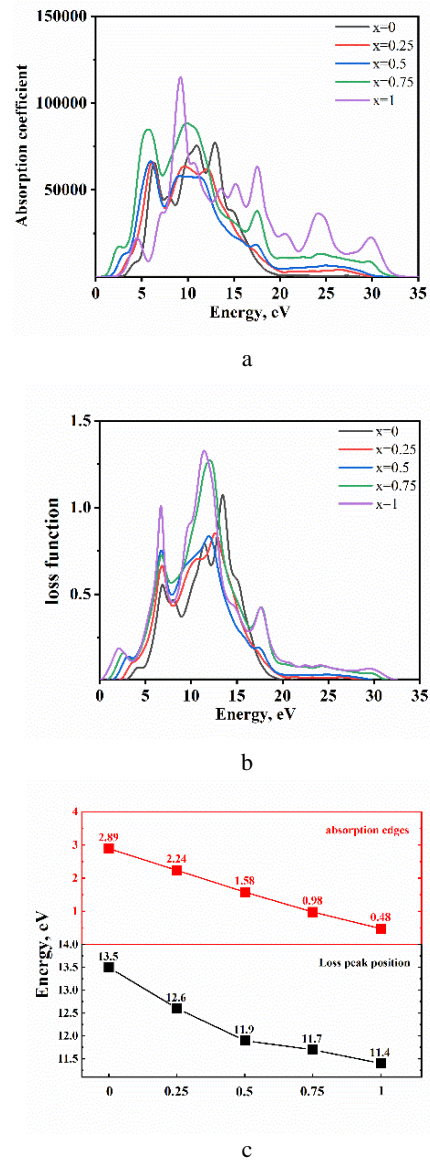

Fig. 6. a – light absorption coefficient; b – light loss; c – light absorption edge and light loss peak position

4. CONCLUSIONS

In this paper, we constructed the AlN and InN monolayer unit cells and calculated the optimized photoelectric characteristics firstly, and then calculated the electrical structure and photoelectric characteristics of $In_xAl_{1-x}N$ with different In densities. In the band structure, with the increase of In atomic composition, the monolayer lattice constant gradually becomes larger, which conforms to Vegard's Law [24]. The bandgap from the AlN monolayer to InN monolayer continuously changes between 2.561 eV and 1.936 eV. By adjusting the composition of In and Al, the forbidden bandwidth of the $In_xAl_{1-x}N$ monolayer is directly and continuously adjustable in the forbidden bandwidth of AlN and InN, which realizes the application of $In_xAl_{1-x}N$ materials from visible light to ultraviolet light.

In optical properties, with the increase of In, the static dielectric constant gradually increases, and the transition ability of electrons gradually increases, making it easier for electrons to transition from the top of the valence band to

the lower conduction band, and five in the imaginary part of the complex dielectric function. The peak of the curve has a redshift, and the peak moves in the direction of low energy. From the light absorption and loss diagram, we can observe that the light absorption spectrum is analogous to the change of the bandgap. In the two-dimensional $In_xAl_{1-x}N$ monolayer, InN has the highest absorption peak, and AlN has the lowest peak. At the same, with the gradual increase of In composition, the absorption peak intensity of two-dimensional $In_xAl_{1-x}N$ increases. All of these show that the In component can introduce light absorption to improve the luminescence performance of $In_xAl_{1-x}N$, which is beneficial to the development of optoelectronic devices.

Acknowledgments

REFERENCES

1. **Bagavath, C., Nasi, L., Kumar, J.** Investigations on the Nanostructures of GaN, InN and $In_xGa_{1-x}N$ *Materials Science in Semiconductor Processing* 49 2016: pp. 61–67. https://doi.org/10.1016/j.mssp.2016.03.032

2. **Mi, M., Zhang, M., Wu, S., Yang, L., Hou, B., Zhou, Y., Guo, L., Ma, X., Hao, Y.** High Performance InAlN/GaN High Electron Mobility Transistors for Low Voltage Applications *Chinese Physics B* 29 (5) 2020: pp. 57307–57307. https://doi.org/10.1088/1674-1056/ab821e

3. **Li, R., Fei, W., Tang, R., Wu, Z., Duan, C., Zhang, T., Zhu, D., Zhang, W., Zhao, S.** Investigation on Threshold Voltage of p-channel GaN MOSFETs Based on p-GaN/AlGaN/GaN heterostructure *Chinese Physics B* 30 (8) 2021: pp. 87305–87305. https://doi.org/10.1088/1674-1056/ac0793

4. **Wang, X., Li, Z., Zhai, C., Ma, J., Duan, Y., Gao, H.** Growth and Characterization of $In_xAl_{1-x}N$ films on silicon substrate by magnetron sputtering method *Materials Research Express* 6 2018: pp. 024615–024615. https://doi.org/10.1088/2053-1591/aaef0d

5. **Teles, L. K., Scolfaro, L., Leite, J. R., Furthmüller, J., Bechstedt, F.** Phase Diagram, Chemical Bonds, and Gap Bowing of Cubic $In_xAl_{1-x}N$ Alloys: Ab Initio Calculations *Journal of Applied Physics* 92 (12) 2002: pp. 7109–7113. https://doi.org/10.1063/1.1518136

6. **Teles, L. K., Furthmüller, J., Scolfaro, L., Tabata, A., Leite, J. R., Bechstedt, F., Frey, T., As, D. J., Lischka, K.** Phase Separation and Gap Bowing in Zinc-blende InGaN, InAlN, BGaN, and BAlN Alloy Layers *Physica E: Low-dimensional Systems and Nanostructures* 13 (2–4) 2002: pp. 1086–1089. https://doi.org/10.1016/S1386-9477(02)00309-0

7. **Deibuk, V.G., Voznyi, A. V.** Thermodynamic Stability and Redistribution of Charges in Ternary AlGaN, InGaN, and InAlN Alloys *Semiconductors* 39 (6) 2005: pp. 623–628. https://doi.org/10.1134/1.1944849

8. **Lepkowski, S.P., Gorczyca, I.** Elastic Properties of InGaN and InAlN from First-principles Calculations *Physics of Semiconductors* 1566 2013: pp. 83–84. https://doi.org/10.1063/1.4848296

9. **Akcay, A., Gokoglu, G., Ersan, F., Akturk, E.** Interactions of h-AlN Monolayer with Platinum, Oxygen, and their Clusters *Chemical Physics: A* 455 2015: pp. 73–73.

https://doi.org/10.1016/j.chemphys.2015.03.012

10. **Sun, X., Yang, Q., Meng, R., Tan, C. J., Liang, Q., Jiang, J., Ye, H., Cheng, X.** Adsorption of Gas Molecules on Graphene-like InN Monolayer: A First-principle Study *Applied Surface Science* 404 (15) 2017: pp. 291–299. https://doi.org/10.1016/j.apsusc.2017.01.264

11. **Beiranvand, R.** Electronic and Magnetic Properties of Cd-doped Zigzag AlN Nanoribbons from First Principles *Rare Metals* 35 (10) 2016: pp. 771–778. https://doi.org/10.1007/s12598-015-0471-z

12. **Zhang, H., Sun, X., Guo, J., Li, Z. C.** Preparation and Characterization of Nanostructured Ni_2N Thin Film as Electrode for Lithium Ion Storage *Applied Surface Science* 420 2017: pp. 196–204. https://doi.org/10.1016/j.apsusc.2017.05.139

13. **Liu, X., Zhang, Z., Lv, B., Ding, Z., Luo, Z.** The External Electric Field-Induced Tunability of the Schottky Barrier Height in Graphene/AlN Interface: A Study by First-Principles *Nanomaterials* 10 (9) 2020: pp. 1794–1794. https://doi.org/10.3390/nano10091794

14. **Liu, X., Zhang, Z., Lv, B., Ding, Z., Luo, Z.** Impact of the Vertical Strain on the Schottky Barrier Height for Graphene/AlN Heterojunction: A Study by the First-principles Method *The European Physical Journal B: Condensed Matter and Complex Systems* 94(1) 2021: pp. 941–947. https://doi.org/10.1140/epjb/s10051-020-00010-w

15. **Ouyang, T., Qian, Z., Ahuja, R., Liu, X. F.** First-principles Investigation of CO Adsorption on Pristine, C-doped and N-Vacancy Defected Hexagonal AlN Nanosheets *Applied Surface Science* 439 (1) 2018: pp. 196–201. https://doi.org/10.1016/j.apsusc.2018.01.040

16. **Zhang, J. Y., Liou, B. T., Lin, H. W., Shi, Y. H., Kuo, Y. K.** Numerical Investigation on the Enhanced Carrier Collection Efficiency of Ga-face GaN/InGaNp-i-n Solar Cells with Polarization Compensation Interlayers *Optics Letters* 36 (17) 2011: pp. 3500–3500. https://doi.org/10.1364/OL.36.003500

17. **Chung, K., Lee, C. H., Yi, G. C.** Transferable GaN Layers Grown on ZnO-Coated Graphene Layers for Optoelectronic Devices *Science* 330 (6004) 2010: pp. 655–657. https://doi.org/10.1126/science.1195403

18. **Gonschorek, M., Carlin, J. F., Feltin, E., Py, M. A., Grandjean, N.** Self-assembly of Silver Nanoparticles: Synthesis, Stabilization, Optical Properties, and Application in Surface-enhanced Raman Scattering *Journal of Applied Physics* 109 (6) 2011: pp. 510–510. https://doi.org/10.1063/1.3552932

19. **Holzworth, M. R., Rudawski, N. G., Pearton, S. J., Jones, K. S., Lu, L., Kang, T. S., Ren, F., Johnson, J. W.** Characterization of the Gate Oxide of an AlGaN/GaN High Electron Mobility Transistor *Applied Physics Letters* 98 (12) 2011: pp. 122103–122103. https://doi.org/10.1063/1.3569715

20. **Song, J. O., Ha, J. S., Seong, T. Y.** Ohmic-Contact Technology for GaN-Based Light-Emitting Diodes: Role of P-Type Contact *IEEE Transactions on Electron Devices* 57 (1) 2010: pp. 42–59. https://doi.org/10.1109/TED.2009.2034506

21. **Akazawa, M., Gao, B., Hashizume, T., Hiroki, M., Yamahata, S., Shigekawa, N., Wetzel, C., Khan, A.** Investigation of Polarization-induced Electric Field in Ultrathin InAlN Layers on GaN by X-ray Photoelectron Spectroscopy *Physica Status Solid C* 8 (7–8) 2011: pp. 2139–2141.

https://doi.org/10.1002/pssc.201000917

22. **He, H., Cao, Y. G., Fu, R. L., Guo, W., Huang, Z., Wang, M. L., Huang, C. G., Huang, J. Q., Wang, H.** Band Gap Energy and Bowing Parameter of In-rich InAlN Films Grown by Magnetron Sputtering *Applied Surface Science* 256 (6) 2010: pp. 1812 – 1816.
https://doi.org/10.1016/j.apsusc.2009.10.012

23. **Ding, Z. Y.** Effect of AlN Coating on Hydrogen Permeability and Surface Structure of VT6 Alloy by Vacuum Arc Ion Plating *Chinese Physics B* 28 (10) 2019: pp. 108101 – 108101.
https://doi.org/CNKI:SUN:ZGWL.0.2019-10-073

24. **Capron, N., Carniato, S., Boureau, G., Pasturel, A.** Study of Oxygen Vacancies in Silica Using Ultra Soft Pseudopotentials *Journal of Non-Crystalline Solids* 245 (1 – 3) 1999: pp. 146 – 149.
https://doi.org/10.1016/S0022-3093(98)00858-8

25. **Whetten, R. L., Cox, D. M., Trevor, D. J., Kaldor, A.** Correspondence between Electron Binding Energy and Chemisorption Reactivity of Iron Clusters *Physical Review Letters* 54 (14) 1985: pp. 1494 – 1497.
https://doi.org/10.1103/PhysRevLett.54.1494

26. **Nahory, R. E., Pollack, M. A., Johnston, W. D., Barns, R. L.** Band Gap Versus Composition and Demonstration of Vegard's Law for $In_{1-x}Ga_xAs_yP_{1-y}$ Lattice Matched to InP *Applied Physics Letters* 33 (7) 1978: pp. 659 – 661.
https://doi.org/10.1063/1.90455

27. **Ahin, H., Cahangirov, S., Topsakal, M., Bekaroglu, E., Ciraci, S.** Monolayer Honeycomb Structures of Group-IV Elements and III-V Binary Compounds: First-principles Calculations *Physical Review B* 80 (15) 2009: pp. 155453 – 155453.
https://doi.org/10.1103/PhysRevB.80.155453

28. **Shaaban, E. R., Lohner, T., Petrik, P., Khánh, N. Q., Fried, M., Polgár, O., Gyulai, J.** Determination of the Complex Dielectric Function of Ion Implanted Amorphous SiC by Spectroscopic Ellipsometry *Physica Status Solidi* 195 (1) 2010: pp. 277 – 281.
https://doi.org/10.3390/coatings10050480

29. **Löper, P., Stuckelberger, M., Niesen, B., Werner, J., Filipič, M., Moon, S. J., Yum, J. H., Topič, M., De, W. S., Ballif, C.** Complex Refractive Index Spectra of CH3NH3PbI3 Perovskite Thin Films Determined by Spectroscopic Ellipsometry and Spectrophotometry *Journal of Physical Chemistry Letters* 6 (1) 2015: pp. 66 – 71.
https://doi.org/10.1021/jz502471h

30. **Peiponen, K. E., Saarinen, J. J.** Generalized Kramers–Kronig Relations in Nonlinear Optical- and THz-Spectroscopy *Reports on Progress in Physics* 72 (5) 2009: pp. 56401 – 56401.
https://doi.org/10.1088/0034-4885/72/5/056401